Technical Report BU-CS-TR-2001-022

A shorter version of this paper is published in the proceedings of

Face and Gesture Recognition, 2002

An Appearance-Based Framework for 3D Hand Shape Classification and Camera Viewpoint Estimation

Vassilis Athitsos and Stan Sclaroff

Computer Science Department
Boston University
111 Cummington Street
Boston, MA 02215
e-mail {athitsos,sclaroff}@cs.bu.edu

Abstract

An appearance-based framework for 3D hand shape classification and simultaneous camera viewpoint estimation is presented. Given an input image of a segmented hand, the most similar matches from a large database of synthetic hand images are retrieved. The ground truth labels of those matches, containing hand shape and camera viewpoint information, are returned by the system as estimates for the input image. Database retrieval is done hierarchically, by first quickly rejecting the vast majority of all database views, and then ranking the remaining candidates in order of similarity to the input. Four different similarity measures are employed, based on edge location, edge orientation, finger location and geometric moments.

1 Introduction

Techniques that allow computers to understand the shape of a human hand in images and video sequences can be used in a wide range of applications. Some examples are human-machine interfaces, automatic recognition of signed languages and gestural communication, non-intrusive motion capture systems, video compression of gesture content, and video indexing.

Different levels of accuracy are needed by different applications. In certain domains it suffices to recognize a few different shapes, observed always from the same viewpoint. Appearance-based methods are well-suited to that task [24, 14, 6]. On the other hand, 3D hand pose estimation can be useful or necessary in various applications related to sign language recognition, virtual reality, biometrics, and motion capture. Currently, systems requiring accurate 3D hand parameters tend to use magnetic tracking devices and other non vision-based methods [15, 16, 20]. Computer vision systems that estimate 3D hand pose do it only in the context of tracking [18, 7, 27, 21] . In that context, the pose can be estimated at the current frame as long as the system knows the pose in the previous frame. The limitation of tracking methods is that they do not address the issue of estimating 3D pose when information about the previous frame is not available. Because of that limitation, current 3D hand trackers need to be manually initialized and they cannot recover when they lose the track. Developing methods to estimate 3D hand pose from a single frame can lead to hand trackers that are fully automatic and can recover from mistakes, and that is one of the goals of our approach.

A real-time system that tracks 3D hand pose is presented in [21]. That system uses a database of synthetic views and an appearance-based method to retrieve the closest matches to the observed input. To achieve the retrieval time and accuracy that are required for a real-time system, that method only considers database views that correspond to poses near the estimated hand parameters of the previous frame.

In [19], the system aims to recover hand pose from a single image using a machine learning approach, the specialized mappings architecture (SMA). The relationship between hand images and hand poses is one-to-many, meaning that a given hand image could come from different hand poses. In the SMA framework this issue is addressed by learning tens of different functions, that map feature vectors to hand poses. Intuitively, each learned function is a “specialist” that works well if the underlying pose is in a specific region of the output space (i.e. the 3D pose space). Given an input image, we obtain the estimates of all functions. Using computer graphics a synthetic hand image is generated based on each estimate, and the similarity between that image and the input image can be used to choose the best estimate.

One weakness of that system is that it requires its input space to be relatively low-dimensional (with fewer than 20 dimensions). It is still an open question whether such a low-dimensional representation of hand images exists, that carries enough information to identify 3D hand pose. In order to satisfy the low-dimensionality requirement, the input space of the specialized functions is the seven Hu moments of the input image. It can be seen in the experimental results for that system that representing the input image using Hu moments discards a lot of discriminative information that could help find the correct pose.

In this paper we describe a method for estimating 3D hand shape and orientation by retrieving appearance-based matches from a large database of synthetic views. The hand shape in the input image is assumed to be close to one of 26 predefined shapes (Figure 2). The database views are computer-generated renderings of the 26 hand shape prototypes from viewpoints that are sampled uniformly along the surface of the viewing sphere. The advantage of using appearance-based matching for 3D parameter estimation is that the estimation is done indirectly, by looking up the ground truth labels of the retrieved synthetic views. This way we avoid the ill-posed problem of recovering depth information directly from the input image.

Our framework has two main advantages over previous appearance-based methods for hand shape recognition [17, 23, 5, 26]: it can handle images from arbitrary viewpoints, and, in addition to classifying hand shape, it provides estimates for the camera orientation. In [1] we presented an early implementation of our framework, in which the chamfer distance ([3]) between edge images was used to estimate similarity between the input image and the database views. In this paper we present additional similarity measures (Section 3), we introduce a method to combine different measures, and we describe a hierarchical retrieval algorithm that first quickly rejects the vast majority of the database views and then ranks the remaining views in order of similarity to the input (Section 5). Compared to the approach described in [1], experiments with our current system demonstrate higher accuracy and vast improvements in retrieval time.

2 Proposed Framework

We model the hand as an articulated object, consisting of 16 links: the palm and 15 links corresponding to finger parts. Each finger has three links (Figure 1). There are 15 joints, each connecting a pair of links. The five joints connecting fingers to the palm allow rotation with two degrees of freedom (DOFs), whereas the 10 joints between finger links allow rotation with one DOF. Therefore, a total of 20 DOFs describes completely all degrees of freedom in the joint angles. For the 20-dimensional vector containing those 20 DOFs we use synonymously the terms “internal hand parameters,” “hand shape” and “hand configuration.”

The appearance of a hand shape also depends on the camera parameters. To keep our model simple, we assume that hand appearance depends only on the camera viewing direction (two DOFs), and on the camera orientation (up vector, or image plane orientation) that defines the direction from the center of the image to the top of the image (one DOF). We use the terms “camera parameters,” “external parameters,” and “viewing parameters” synonymously to denote the three-dimensional vector describing viewing direction and camera orientation. Figure 4 illustrates the definition of camera parameters.

Given a hand configuration vector $C = (c_1, ..., c_{20})$ and a viewing parameter vector

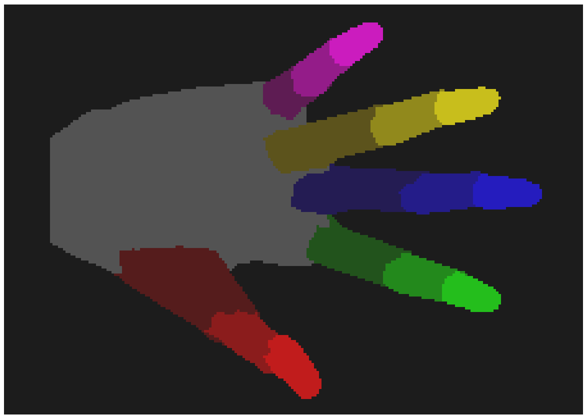

Figure 1: The hand as an articulated object. The palm and each finger are shown in a different color. The three different links of each finger are shown using different intensities of the same color.

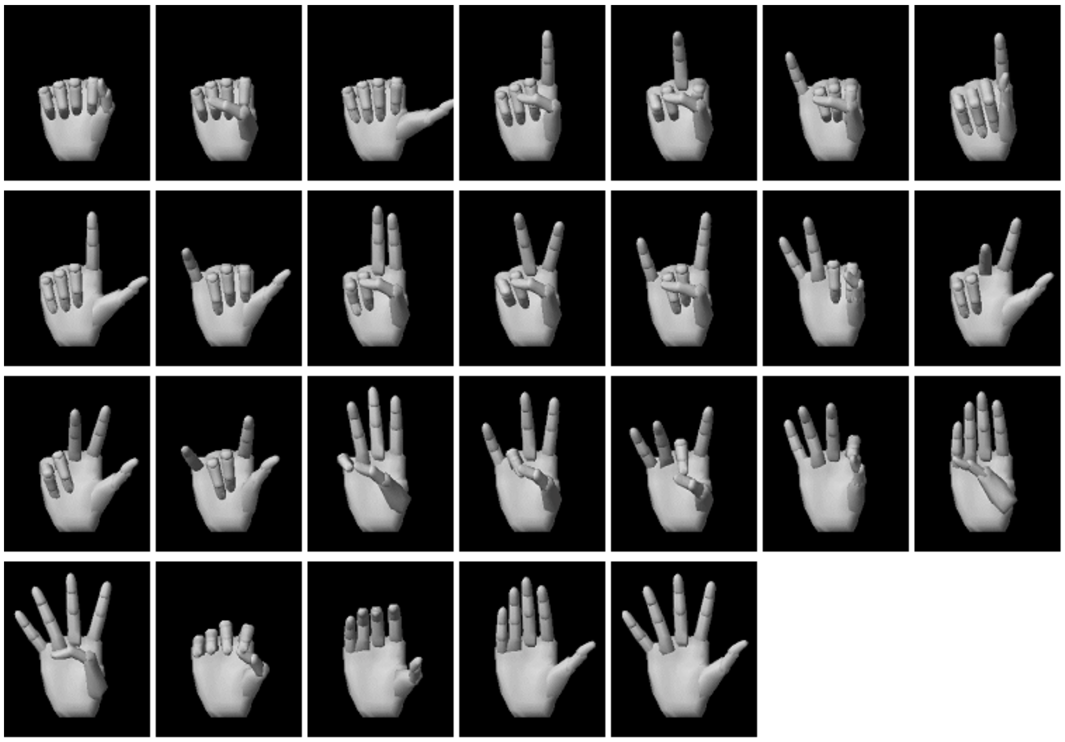

Figure 2: The 26 basic shapes used to generate training views in our database.

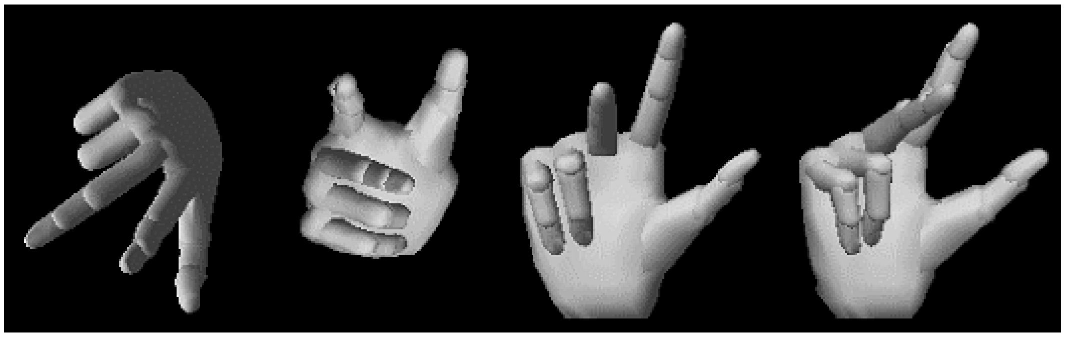

Figure 3: Four different database views of the same basic shape.

$V = (v_1, v_2, v_3)$, we define the hand pose vector P to be the 23-dimensional concatenation of C and V: $P = (c_1, ..., c_{20}, v_1, v_2, v_3)$.

Using these definitions, the generic framework that we propose for hand pose estimation is the following:

1. Preprocessing step: create a database containing a uniform sampling of all possible views of the hand shapes that we want to recognize. Label each view with the hand pose parameters that generated it.

2. For each novel image, retrieve the database views that are the most similar. Use the parameters of the N most similar views as initial estimates for the image.

3. Refine each of the retrieved parameter estimates to optimally match the input.

Our framework allows for systems that return multiple estimates. Multiple estimates can be useful when, either because of deficiencies of the similarity measure, or because of adverse viewing conditions, the retrieval method fails to rank one of the correct matches as the best overall match. If a system returns multiple estimates, we consider the retrieval successful if at least one of those estimates is close to the true parameters of the observed hand. A low value of N may be adequate in domains like 3D hand tracking and sign language recognition, where additional contextual information can be used to discriminate among the returned estimates.

In [1] we speculate on the possibility of using this framework to estimate arbitrary hand shapes, by including a lot of hand shape prototypes in the database, so that for any possible observed shape there is a “close enough” shape in the database. In this paper we tackle an easier version of the problem, by assuming that the observed hand shape is close to one of 26 shape prototypes. We also ignore step 3 of the framework, i.e. the refinement process.

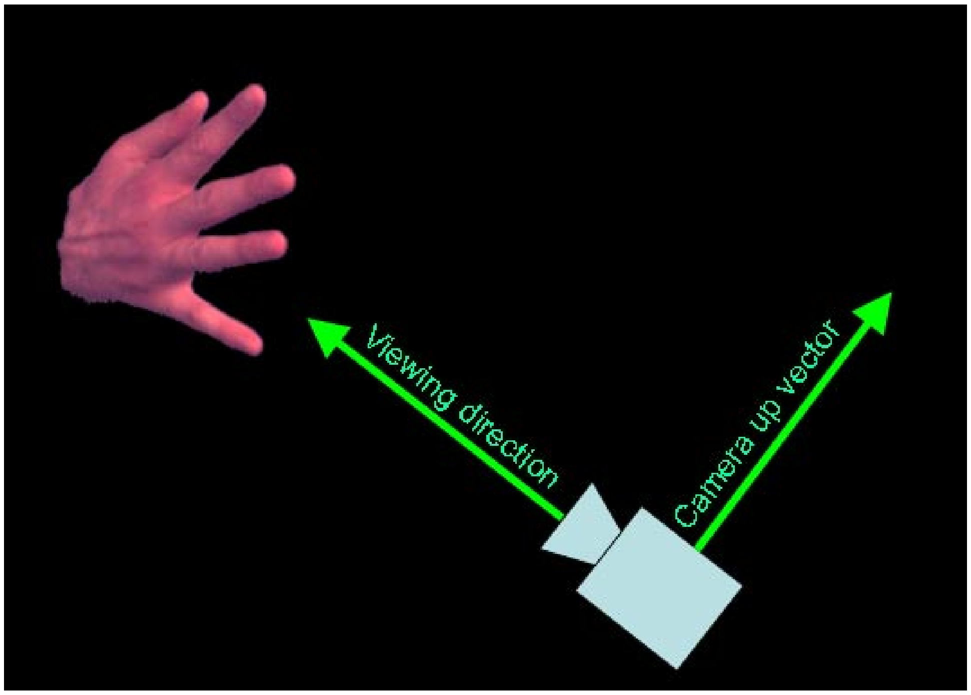

Figure 4: The viewing direction is the line connecting the camera's center of projection to the center of the hand. The camera up vector defines the rotation of the camera, which specifies the upward direction on the image plane. The camera “up” vector is constrained to be on the plane that is perpendicular to the viewing direction.

3 Similarity Measures

To retrieve the most similar database views for an input image we combine four different similarity measures: Edge location similarity, edge orientation similarity, finger-based matching, and matching based on central and Hu moments. This section describes the individual measures. Section 5 discusses how those measures are combined.

3.1 Chamfer Distance

We define the distance D between a point p and a set of points X to be the Euclidean distance between p and the point in X that is the closest to p:

$$D(p, X) = \min_{x \in X} ||p - x|| \tag{1}$$

The directed chamfer distance between two sets of points X and Y is defined in [3]. In our system we use the undirected chamfer distance D_c, defined as follows:

$$D_c(X, Y) = \frac{1}{|X|} \sum_{x \in X} D(x, Y) + \frac{1}{|Y|} \sum_{y \in Y} D(y, X) \tag{2}$$

We use D_c to measure the distance between the edge image of the input and the edge image of a database view. Edge images are represented as sets of edge pixels. Before we apply D_c we normalize the scale of both edge images, so that the longest sides of their bounding boxes are equal. The advantage of D_c over the directed chamfer distance is that D_c, in addition to penalizing for points in X that have no close match in Y, it also penalizes for points in Y that have no close match in X. In general, the chamfer distance is relatively robust to small translations, rotations and deformations of the test image with respect to the corresponding model image.

For the synthetic views, edge extraction can be done in a noise-free way. Each pixel is labeled with the link that it belongs to. A border between different links is considered to be an edge, unless it is identified with a joint connecting neigbboring links. In our input images such borders that correspond to joints do not give rise to particularly strong edges.

Real images used for testing are preprocessed by segmenting the hand using skin detection [13], and by normalizing the scale of the segmented hand. Edges are extracted using a Canny detector, implemented in Intel's OpenCV programming library [12].

3.2 Edge Orientation Histograms

Given a gray-scale image I, and its corresponding edge image E, we define the orientation R of an edge pixel p to be $R(p) = \arctan \frac{I_y(p)}{I_x(p)}$, where I_x, I_y are the image gradients along the x and y directions. Orientation values are between 0 and 180 degrees. We store those orientation values in an edge orientation histogram with 96 bins, normalized so that the sum of all bin values is 1. We denote the i-th bin of histogram H as $B(H, i)$. In general, if k is the number of bins, and b is the index of one of the bins, we define the cumulative histogram $C(H, b)$ by the formula

$$B(C(H,b),i) = \sum_{j=b}^{b+i} B(H, j \bmod k) \tag{3}$$

As a similarity measure between edge orientation histograms we use the maximum cumulative histogram intersection. The histogram intersection S'_h of histograms H and J is defined in [22] as

$$S'_h(H,J) = \sum_{i=0}^{k-1} \min(B(H,i), B(J,i)) \tag{4}$$

We define the maximum cumulative histogram intersection $S_h(H, J)$ as

$$S_h(H,J) = \max_{0<=b<k} S'_h(C(H,b), C(J,b)) \tag{5}$$

Using cumulative histograms in histogram intersection makes the measure less sensitive to small orientation changes in an image. For example, consider the case where we have three histograms H, J, K, such that $B(H,0) = 1, B(J,1) = 1, B(K,48) = 1$ and all the other bins of H, J and K are zero. Then, histogram intersection applied directly to those histograms would find that H is equally dissimilar to J and to K, since $S'_h(H, J) = S'_h(H, K) = 0$. Intuitively we would like the similarity measure to find that H and J are very similar, whereas H and K are very different. After all, if an image has an edge orientation histogram equal to H, rotating that image by a mere two degrees may cause its histogram to be equal to J, whereas only a rotation close to 90 degrees would make its histogram equal to K. If we apply histogram intersection to the cumulative versions of H, J and K we get the desired result, that H is very similar to J and very different from K. In particular, $S'_h(C(H,0), C(J,0)) = k - 1$ whereas $S'_h(C(H,0), C(K,0) = k - 48$. Note that the maximum similarity value that can be returned by S'_h is k, i.e. the number of bins, which is 96 in our system.

The reason we don't simply define $S_h(H, J)$ to be $S'_h(C(H,0), C(J,0))$ is that edge orientation histograms are circular; orientation values corresponding to bin 0 are as close to values corresponding to bin 1 as to those corresponding to bin $k - 1$. One example that illustrates the advantages of using S_h is the following: consider a case where three histograms, H, J, and K, are such that $B(H,0) = 1, B(J,k-1) = 1, B(K,1) = 1$, and all other bins of H, J and K are 0. In that case, $S'_h(C(H,0), C(J,0)) = 1$, and $S'_h(C(H,0), C(K,0)) = k - 1$. Note that, intuitively, H should be equally similar to both J and K, since equal amounts of image plane rotation can change H into either J or K. S'_h clearly does not behave as desired in this case, but S_h does the right thing, since $S_h(H, J) = S_h(H, K) = 1$.

3.3 Finger Matching

Given the binary image of a hand, most significant protrusions that we observe are caused by fingers (Figures 2, 3, 9). We can easily detect such protrusions and use them to define a similarity measure between hand images. In Section 4 we describe how protruding fingers are detected. Here we define a similarity measure between hand images that is based on protruding fingers.

We represent a protrusion F as the ordered triple (P_F, A_F, B_F) where P_F is the fingertip point, and A_F, B_F are the endpoints of the boundary contour of the protrusion. We define the *base point* Q_F of F as the middle point of the straight line segment between A_F and B_F (Figure 5). Our finger detector identifies protrusions whose width is less than a threshold T_w and whose elongation exceeds a threshold T_e.

The length of a contour segment is defined to be the number of pixels along that segment. The length $L(F)$ of protrusion F is defined as the minimum of the lengths of the segments $A_F P_F$ and $P_F B_F$. The width $W(F)$ of F is the symmetric Hausdorff distance ([9]) between the contour segments $A_F P_F$ and $P_F B_F$. If $X = A_F P_F$ and $Y = P_F B_F$, then

$$W(F) = \max(\max_{x \in X} D(x, Y), \max_{y \in Y} D(y, X)) \tag{6}$$

using the point-to-set distance D defined in Equation 1. The elongation E of a protrusion F is defined as $E(F) = \frac{L(F)}{W(F)}$.

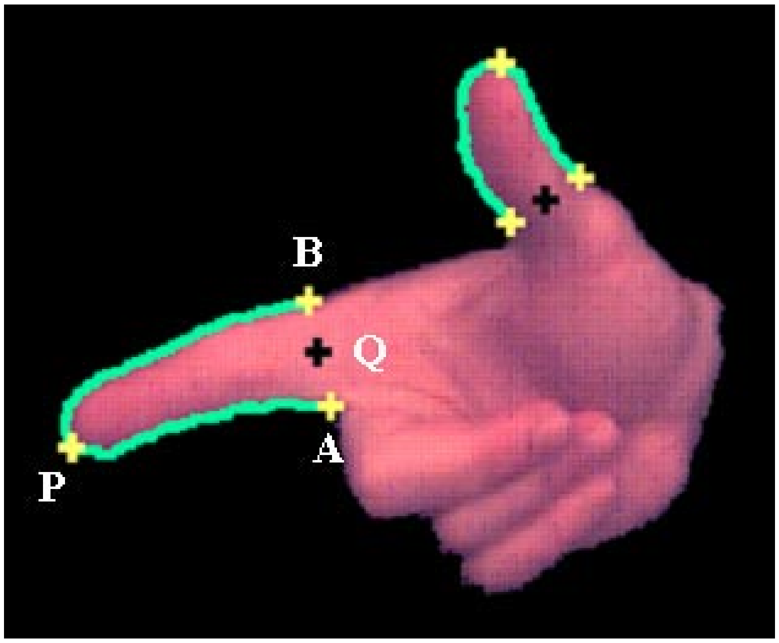

Figure 5: An example output of the finger detector. For the index finger, P is the fingertip, A and B are the boundary endpoints of the finger and Q is the base point. The contour segments AP and PB are shown in green.

In defining a distance measure between hand images that uses the results of finger detection, we need to have in mind that a slight change in hand shape or camera viewpoint can cause the elongation of a finger to drop below the detection threshold T_e. Because of that, we generate two sets of fingers for a given hand image I: a set of *definite* fingers S_d^I, detected by setting $T_e = 1.8$, and a set of *potential* fingers S_p^I, detected with $T_e = 1.1$. Protrusions whose elongation exceeds 1.8 are almost always fingers, so labeling them as fingers we get very few false positives. At the same time, if a finger has elongation over 1.8 in a synthetic or real image of a given hand shape from a given viewpoint, it is a pretty safe bet that in other images of the same shape from a similar viewpoint that finger will have an elongation of at least 1.1. Therefore, labeling protrusions whose elongation is over 1.1 as fingers we get very few false negatives. A finger-based similarity/distance measure between two images should penalize for definite fingers in one image that have no corresponding (i.e similar in location and orientation) potential fingers in the other image.

Another consideration in defining a finger-based similarity measure is that a slight change in hand shape or viewpoint can cause two protruding fingers to be detected as a single protrusion. Therefore, the similarity measure should not require one-to-one matching between fingers; it should give high similarity (low distance) values as long as for each definite finger in one image there is a similar potential finger in the other image, even if a finger in one image is matched to more than one fingers in the other image.

We define the distance between fingers F and G to be

$$\|F - G\| = \max(\|P_F - P_G\|, \|Q_F - Q_G\|) \tag{7}$$

The finger-based distance D_f between an input image I and a database view V is defined as

$$D_f(I, V) = \max(\max_{F \in S_d^I}\{D(F, S_p^V)\}, \max_{G \in S_d^V}\{D(G, S_p^I)\}) \tag{8}$$

using the point-to-set distance D defined in Equation 1 and the finger distance defined in Equation 7.

Intuitively, D_f penalizes for any “definite” finger in either image for which there is no nearby “potential” finger in the other image. It does not penalize for any “potential” finger in one image that has no close match in the other image. Before we apply D_f on two hand images, we center them and normalize their scale, as described in the subsection on the chamfer distance.

It may turn out that a more sophisticated finger-based similarity measure can give more accurate results than the ones reported in Section 6 using D_f. For example, it may be beneficial to explicitly take into account differences in length, width, elongation and orientation in the distance between fingers defined in Equation 7. In addition, we could modify D_f to require that if two fingers are far enough from each other in one image they should be matched to different fingers in the other image.

3.4 Moment-Based Matching

From a hand image I we compute seven central moments and seven Hu moments ([8]), and store them in a 14-dimensional moment vector. We perform Principal Component Analysis ([4]) on the moment vectors of all database views, and we identify the top nine eigenvectors. We define the moment-based distance D_m between an input image I and a database view V to be the Mahalanobis distance ([4]) between their moment vectors, after they have been projected to the eigenspace spanned by the top nine eigenvectors.

4 Detection of Protruding Fingers

Looking at images of segmented hands we notice that most significant contour protrusions correspond to fingers. Based on this observation, we have implemented a simple detector of protruding fingers, whose results are used in the finger-based similarity measure described in Section 3.3. The detector essentially identifies protrusions whose width and length are within a specified range. This section describes in detail how the detector works. Readers interested in the general framework of our system may prefer to skip this section; we include it to facilitate duplication of our results by other implementations.

The main steps in identifying protruding fingers are the following:

1. Find the bounding contour of the hand.

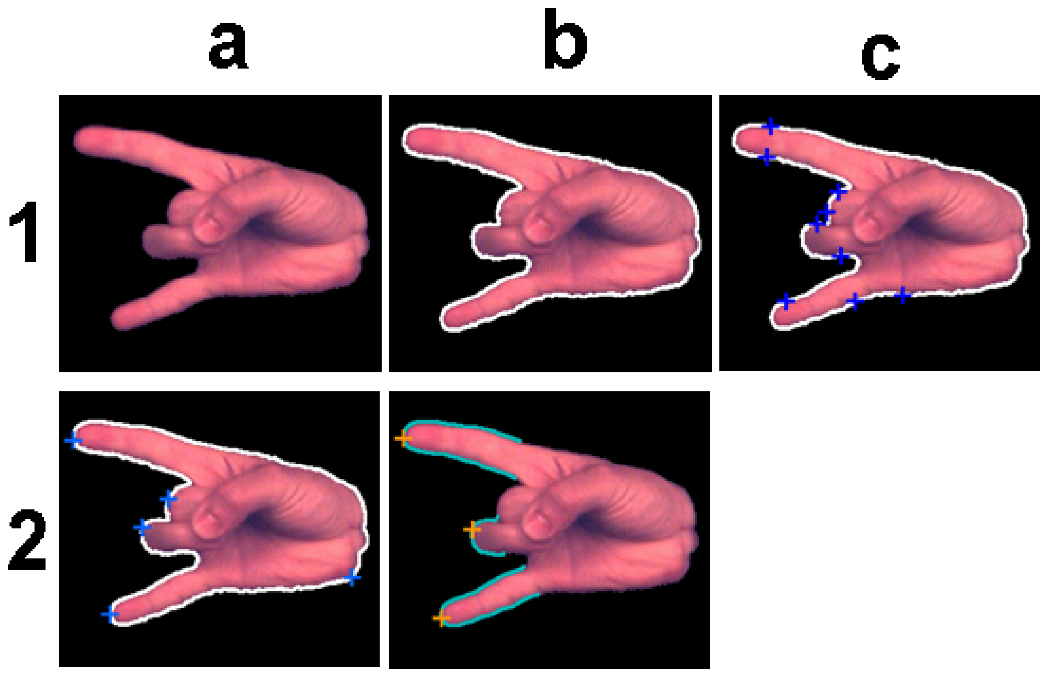

Figure 6: Illustrations of some of the steps our finger detector goes through. 1a) The input image. 1b) The bounding contour is indicated in white. 1c) Inflection points are indicated as blue crosses on the contour. 2a) Points of negative maximal curvature are indicated as blue crosses on the contour. 2b) The contour of detected fingers is indicated in blue. The fingertips are indicated in orange.

2. Find inflection points, where the curvature of the contour changes sign.

3. Find points of negative maximal curvature. Each of those points must have the highest curvature in the contour segment between two consecutive inflection points, and its curvature must be negative.

4. For each point of negative maximal curvature, consider it a tip of a protrusion, and measure the width, length and elongation (length/width ratio) of that protrusion.

5. Label as fingers all protrusions that are large enough and whose elongation exceeds a specified threshold.

Figure 6 illustrates some of the steps described above.

The input to the finger detector is the segmented image of the hand. The image gets rescaled, so that the bounding square of the hand is 192x192 pixels. Then, the boundary contour is located, and represented as a sequence of k pixels $(P_0, P_1, ..., P_{k-1})$ such that P_i is a neighbor of P_{i-1} and P_{i+1}, and P_0 is a neighbor of P_{k-1}. Each pixel P_i is represented by its image coordinates (x_i, y_i). The contour is smoothed, by replacing each pixel P_i with the pixel in the midpoint between P_{i-3} and P_{i+3}.

In the smoothed contour we identify points of inflection, in which the curvature changes sign (Figure 6). The goal of this step is to split the contour into segments in which the curvature tends to maintain its sign (either positive or negative). Those segments are separated by the inflection points. We define the orientation $O(P)$ of the contour at a point P to be the angle between the x axis and the slope of the contour at P. Angles here are measured in radians. We define the curvature of a contour point to be the second derivative of that point. Given a sequence of contour points $P_0, P_1, ..., P_k - 1$, we define the derivative $D(P_i)$ at point P_i to be

$$D(P_i) = \frac{y_{i+10} - y_{i-10}}{x_{i+10} - x_{i-10}} \tag{9}$$

Given a starting point A, to find the next inflection point, we start walking along the contour, until we find a point B at which the contour orientation differs by more than 0.3 radians from the orientation at A. The sign of the difference $O(B) - O(A)$ will be the curvature sign for the current contour segment. The reason we use 0.3 radians as a threshold is that we want the contour segment to have an overall change of orientation of at least 0.3 radians, we don't want to split segments that are more or less straight but along which the curvature fluctuates slightly above and slightly below zero.

After we determine the curvature sign for the current segment, we keep moving along the contour, one pixel at a time, storing at variable C, at each step, the point that we encountered after A whose orientation differs the most from the orientation of A. We keep doing that until we reach a point D such that $|O(D) - O(A)| < |O(C) - O(A)| - 0.3$. At that point the system identifies the pixel stored in C as an inflection point. Basically, the segment CD of the contour has an overall change of orientation of at least 0.3 radians and the sign of its curvature is the opposite of the sign of the curvature along the segment AC, and we know that C was the point where the curvature changed sign.

If we still haven't found an appropriate point D and the overall change in orientation along the contour between A and the current point E exceeds π radians, we designate the current point E to be the endpoint of the current segment, and we treat it as an inflection point. We do this because if the contour keeps curving the same way along the next contour points, the orientation of those points will start approaching that of A. Doing this trick we end up designating some points as inflection points when mathematically speaking they are not inflection points, but the rest of the algorithm ensures that this does not cause any problems in detecting protruding fingers.

After we have found an inflection point, or at least a contour segment endpoint, we start again, from that inflection point, to find the next inflection point, and we repeat the process until we have scanned the entire contour. We have found that the location of the first inflection point identified by this process is sensitive to the location of the initial starting point. To account for that, we start at a random point and we do not record the first two inflection points that we find. The third inflection point T that we encounter is the first one that gets recorded, and the process continues until we make a complete circle and reach that point T again.

By identifying inflection points we split the contour into segments along which the curvature sign can be considered stable. The next step is to find, at each segment, the point at which the magnitude of the curvature is maximal. Those maximal curvature points are potential fingertips when their curvature is negative. To decide if a potential fingertip P is a real fingertip or not, we need to determine if there is a contour segment that starts before P, ends after P, and defines a protrusion that is elongated enough.

A triple of points APB defines a protrusion that starts at A, has P as its point of maximal negative curvature ("tip") and ends at B. For any such protrusion we can define its length, width and elongation as discussed in Section 3.3. The length of a contour segment is defined to be the number of pixels along that segment. The length of protrusion APB is defined as the minumum of the lengths of the segments AP and PB. The width of the protrusion is defined to be the Hausdorff distance (Equation 6) between the points along AP and the points along PB. The elongation of the protrusion is defined as the ratio of its length over its width.

Given a protrusion tip P, we want to find the points A' and B' for which the elongation of $A'PB'$ is maximized. We identify those points in a simple way, by simply examining all possible protrusions APB such that the length of AP and the length of PB are less than a threshold T_l (96 pixels in our implementation) and the length of APB is over 15 pixels. We can measure the width, length and elongation of all such protrusions in time quadratic to T_l using dynamic programming. After we find the points A' and B' that maximize the elongation of $A'PB'$, we consider the protrusion $A'PB'$ to be a finger if its elongation exceeds a given threshold (see Section 3.3 for the elongation thresholds our system uses).

The algorithm we described for finding the endpoints A' and B' of a finger is pretty simple, and it often happens that the endpoints that are found are beyond the actual endpoints of the finger. A simple trick that we use that corrects this behavior most of the times is to start trimming the contour segment at its endpoints, until we find two endpoints for which the line connecting them goes from each endpoint inwards, i.e. towards the interior of the hand (as opposed to going towards the image background). Figure 7 illustrates endpoint trimming.

Finally, after we have trimmed all detected fingers, we check to see if any detected fingers overlap too much with each other. We consider that two fingers overlap too much if their contour segments have more than 15 pixels in common. If two fingers overlap, we reject the least elongated of them.

Figure 8 shows sample outputs of the finger detector. In general, depending on the elongation threshold, there is a large fraction of false positive or false negative detections. As described in Section 3.3, our finger-based distance defined in Equation 7 compensates for the inaccuracy of the detector by detecting fingers twice, once with a large elongation threshold, that leads to very few false positives, and once with a smaller elongation threshold, that leads to very few false negatives.

We didn't spend a lot of time designing our protruding finger detector, and we would not be surprised to find out that other approaches can be simpler, more efficient, and more accurate. If we come upon such methods, it will be a simple process to replace our finger

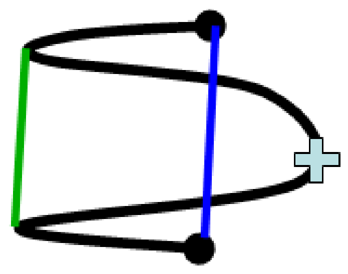

Figure 7: The need for trimming finger endpoints. Suppose that the system has identified the protrusion whose contour segment is indicated by black. The fingertip of the protrusion is indicated by the light blue cross, and the endpoints of the protrusion are the endpoints of the blue line segment. The system can tell that it must trim the protrusion at the endpoints, because the blue line segment, which connects the current endpoints, goes from each endpoint into a background region, before it actually crosses the contour again and enters a foreground region. If we trim the endpoints of the contour as described in the text, the new endpoints of the protrusion will be the endpoints of the green line segment. The green line segment goes from each endpoint into a foreground region (actually, it is entirely inside the foreground region).

detector with them in our system. We described our method here only in order to facilitate duplication of our experiments.

5 Hierarchical Retrieval Using Combinations of Measures

In general, we have found that combining different measures we get more accurate results than by using a single measure. The combination of a set of k measures is done as follows: given an input image I, using each of the measures we can rank the database images in order of similarity to I (the most similar view has rank 1). We denote the rank of the i-th synthetic view V_i under measure j as r_{ij}. We define a new combined measure $M(I, V_i)$ as

$$M(I, V_i) = \sum_{j=1}^{k} (w_j \log r_{ij}) \tag{10}$$

where w_j is a preselected weight associated with the j-th measure. Then, we can rank the synthetic views again, in ascending order of the value that the combined measure M assigned to them. The reason we use in M the *ranks* of a view, as opposed to using the original k measure scores of the view, is that the scores under different measures have different ranges and distributions, and it is not obvious how they should be combined. The rank numbers all belong to the same space and can be easily combined. We sum the logarithms of the ranks, as opposed to the ranks themselves, because this way M behaves more robustly in the frequent cases where a single measure gives a really bad rank to a correct database match.

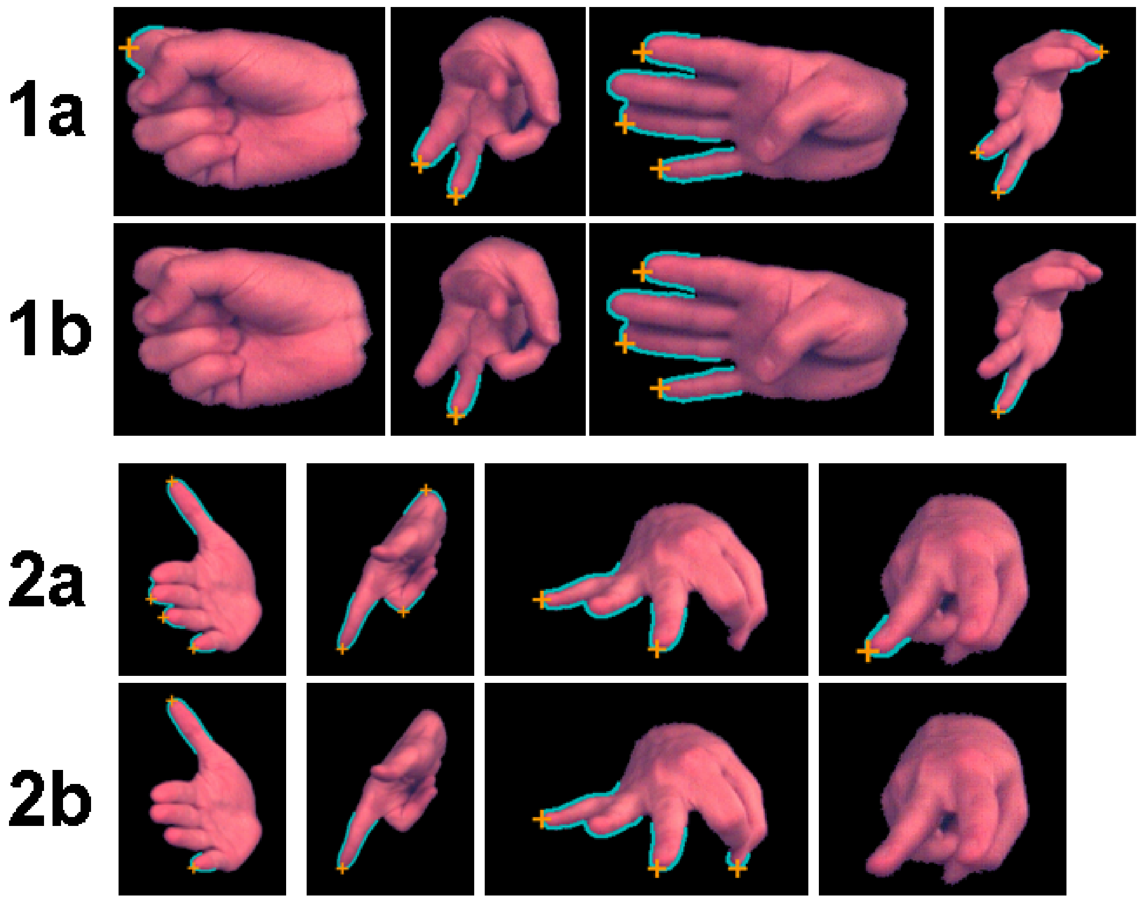

Figure 8: Sample outputs of the finger detector. The elongation threshold was set to 1.1 for rows 1a and 2a, and it was set to 2 for rows 1b and 2b. The contours of detected fingers are shown in blue, and fingertips are marked with orange crosses.

Weights can be tuned to reflect the accuracy and/or redundancy of the individual measures. Our system picks weights automatically by searching over different combinations and choosing the combination that maximizes accuracy over a small training set of real hand images (28 images in our current implementation).

The similarity measures described in section 3 have different strengths and weaknesses. The chamfer distance is the most accurate, but also the most computationally expensive. Moment and finger-based matching, on the other hand, are less accurate, but they can be done almost in real time, if we precompute and save the corresponding features of the database views.

In order for the system to function at more or less interactive speeds, we need a retrieval method that can reject most of the database views very fast, and that applies expensive matching procedures only to a small fraction of likely candidates. Our database retrieval algorithm achieves that using a hierarchical, two-step matching process. First, it ranks the synthetic views by combining finger and moment-based matching, and it rejects the worst-ranking views. This initial screening can be done very fast; it takes under a second in our system. Then, we rank the remaining candidates by combining all four measures. In practice, we have found that retrieval accuracy is only slightly affected if we reject 99% of the views in the screening step. In general, the percentage of views that gets rejected in the first step can be tuned to balance between retrieval speed and accuracy.

6 Experiments

Our database contains renderings of 26 hand shape prototypes (Figure 2). The renderings are done using a commercially available hand rendering programming library ([25]). Each shape is rendered from 86 viewpoints, that constitute an approximately uniform sampling of the surface of the viewing sphere. For each viewpoint we generate 48 database views, using different values for image plane orientation, uniformly spaced between 0 and 360 degrees. Generating multiple rotations of the same image is necessary, since the similarity measures that we use are rotation-variant. Overall, the database contains 4128 views per shape prototype, and 107328 views in total.

We have tested our system with 276 real images displaying the right hands of four different persons. In those images, the hand is segmented using skin detection ([13]). Eight examples of segmented test images are shown in Figure 9. We manually established pseudo-ground truth for each test image, by labeling it with the corresponding shape prototype and using the rendering software to find the viewing parameters under which the shape prototype looked the most similar to the test image. This way of estimating viewpoint parameters is not very exact; we found that estimates by different people varied by 10-30 degrees. Model views can't be aligned perfectly with a test image, because each individual hand has somewhat different finger and palm widths and lengths, and also because the hand shapes in the real images are only approximations of the 26 shape prototypes.

Given the inaccuracy of manual estimates, we consider a database view V to be a *correct match* for a test image I if the shape prototype with which we label I is the one used in generating V, and the manually estimated viewing parameters of I are within 30 degrees of those of V. For any two viewing parameter vectors u and v (see Section 2) there exists a rotation around the center of the viewing sphere that maps u to v. We use the angle of that rotation as the distance between u and v. On average, there are 30.8 correct matches for each test image in the database.

Our measure of the accuracy of the retrieval for a test image is the rank of the *highest-ranking correct match* that was retrieved for that image. 1 is the highest possible rank. A perfect similarity measure, under this definition of accuracy, would always assign rank 1 to one of the correct matches for every test image; it would never assign rank 1 to an incorrect match. Table 1 shows the distribution of the highest ranking correct matches for our test set. We should note that, although the accuracy using the chamfer measure is comparable to the accuracy using the two-step retrieval algorithm, the two-step algorithm is about 100

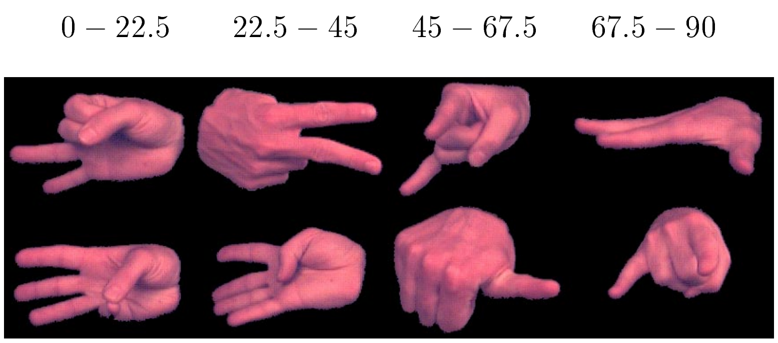

Figure 9: Examples of test images with different frontal angles. The frontal angles of the images in each column belong to the range indicated at the top of that column. Angles here are measured in degrees.

Rank range	Chamfer	Edge hist.	Fingers	Moments	2-step
1	22.8	0.0	7.6	2.5	21.7
1-2	31.9	0.0	11.2	6.5	31.5
1-4	40.9	0.0	18.1	8.6	41.7
1-8	49.6	0.3	26.8	13.4	52.5
1-16	58.3	2.2	34.0	20.3	60.1
1-32	68.8	4.7	43.8	30.1	68.8
1-64	77.5	6.5	50.7	38.0	76.4
1-128	85.9	11.2	56.2	47.5	83.7
1-256	92.0	23.6	68.5	58.0	87.3
257-	8.0	76.4	31.5	42.0	12.7

Table 1: Retrieval accuracy: for each rank range and each measure we indicate the percentage of test images for which the rank of the highest ranking correct match was in the given range. 2-step stands for the two-step retrieval algorithm described in Section 5.

times faster than simply applying the chamfer distance to each database view.

The viewing parameters for the test images were more or less evenly distributed along the surface of the viewing sphere. We call a hand view ”frontal” if the camera viewing direction is almost perpendicular to the palm of the hand, and we call it a ”side view” if the viewing direction is parallel to the palm. The ”frontal angle” of a view is the angle (between 0 and 90 degrees) between the viewing direction and a line perpendicular to the palm. Figure 9 shows some examples of test images with different frontal angles. Table 2 shows the median rank of the highest-ranking correct matches for test images observed from different frontal angle ranges. As expected, retrieval accuracy is worse for side views, where fewer features are visible. It is fair to mention that, in some of the side views, even humans find it hard to determine what the shape is (see Figure 9).

The weights used to combine the finger and moment-based measures (Equation 10) in

Frontal angle	0-22.5	22.5-45	45-67.5	67.5-90
# of images	54	72	86	64
Median	1	3	9	47

Table 2: Accuracy of the two-step retrieval algorithm over different frontal angles. For each range of frontal angles we indicate the number of test images whose frontal angles are in that range and the median of the highest ranking correct matches for those images.

the screening step of the retrieval were 0.6 and 0.4. The weights used in the second step of the retrieval were 0.4 for the chamfer and the finger-based measure, and 0.1 for the edge orientation measure and the moment-based measure. These weights were established using a small training set of 28 real images, none of which was included in the test set.

Retrieval times were between 3 and 4 seconds on a PC with a 1.2GHz Athlon processor. The memory requirements of the system were under 100MB.

7 Future Work

Our long term goal is a system that can provide reliable estimates for arbitrary hand shapes, seen from arbitrary viewpoints, at speeds that allow for interactive applications. In order to do that, we need to include more shape prototypes in the database, and implement the refinement step of the framework presented in Section 2. At the same time we need to work on improving retrieval accuracy. We plan to investigate ways of extracting more information from the input image, using more elaborate bottom-up processing. We are currently looking into methods of detecting fingers and fingertips in the interior of the hand.

As the size of the database grows larger, the issue of retrieval efficiency will become critical. It may take under a second to apply finger and moment-based matching to a database of 100,000 images, but the time may become prohibitive if we use a significantly larger set of hand shape prototypes and the number of views grows into the millions or tens of millions. We need to investigate ways of building index tables, that can automatically focus the search on smaller parts of the database. We are currently developing an indexing scheme that can direct the database search using the locations of detected fingers. Index tables may prove to be feasible even for measures like the chamfer distance or the related Hausdorff distance. [11] describes how to embed the Hausdorff distance into an L_∞ metric and [10] discusses efficient methods for answering approximate nearest neighbor queries in L_∞ spaces.

Another system aspect that we have neglected so far is hand segmentation. In our test images the hand was segmented using skin detection ([13]), but those images were captured using a background that made segmentation relatively easy. It is important to evaluate the performance of our similarity measures under realistic segmentation scenarios and especially in the presence of segmentation errors. As a start, we plan to use our system as the basis for a real-time desktop human computer interface, where the hand is segmented using skin color and motion.

8 Conclusions

We have presented a general framework for 3D hand pose classification from a single image, observed from an arbitrary viewpoint, using appearance-based matching with a database of synthetic views. Using the ground truth labeling of the retrieved images the system can also estimate camera viewing parameters. We use a hierarchical retrieval algorithm, which combines the efficiency of computationally cheap similarity measures with the increased accuracy of more expensive measures, and runs at close to interactive speed.

Acknowledgements

This research was supported in part by the National Science Foundation, under grants IIS-9912573 and EIA-9809340. Any opinions, findings, and conclusions or recommendations expressed in this material are those of the authors and do not necessarily reflect the views of the National Science Foundation.

References

[1] Vassilis Athitsos and Stan Sclaroff. 3D hand pose estimation by finding appearance-based matches in a large database of training views. In *IEEE Workshop on Cues in Communication*, 2001.

[2] Vassilis Athitsos and Stan Sclaroff. An appearance-based framework for 3D hand shape classification and camera viewpoint estimation. Technical Report BU-CS-TR-2001-022, Boston University, December 2001.

[3] H.G. Barrow, J.M. Tenenbaum, R.C. Bolles, and H.C. Wolf. Parametric correspondence and chamfer matching: Two new techniques for image matching. In *IJCAI*, pages 659–663, 1977.

[4] R.O. Duda, P.E. Hart, and D.G. Stork. *Pattern Classification*. Wiley-Interscience, 2001.

[5] W.T. Freeman and M. Roth. Computer vision for computer games. In *Automatic Face and Gesture Recognition*, pages 100–105, 1996.

[6] R. Hamdan, F. Heitz, and L. Thoraval. Gesture localization and recognition using probabilistic visual learning. In *CVPR*, volume 2, pages 98–103, 1999.

[7] T. Heap and D. Hogg. Towards 3D hand tracking using a deformable model. In *Face and Gesture Recognition*, pages 140–145, 1996.

[8] MK Hu. Visual pattern recognition by moment invariants. *IRE Transactions on Information Theory*, IT-8:179–187, 1962.

[9] D. Huttenlocher, D. Klanderman, and A. Rucklige. Comparing images using the Hausdorff distance. *IEEE Transactions on Pattern Analysis and Machine Intelligence*, 15(9):850–863, September 1993.

[10] P. Indyk. On approximate nearest neighbors in non-euclidean spaces. In *FOCS*, pages 148–155, 1998.

[11] P. Indyk. *High-dimensional Computational Geometry*. PhD thesis, Stanford University, 2000.

[12] Intel Corporation. *Open Source Computer Vision Library Reference Manual*, December 2000.

[13] M.J. Jones and J.M. Rehg. Statistical color models with application to skin detection. In *CVPR*, pages I:274–280, 1999.

[14] M. Kohler. Special topics of gesture recognition applied in intelligent home environments. In *Proceedings of the Gesture Workshop*, pages 285–296, 1997.

[15] R. Liang and M. Ouhyoung. A real-time continuous gesture recognition system for sign language. In *Face and Gesture Recognition*, pages 558–567, 1998.

[16] J. Ma, W. Gao, and C. Wang J. Wu. A continuous chinese sign language recognition system. In *Face and Gesture Recognition*, pages 428–433, 2000.

[17] B. Moghaddam and A. Pentland. Probabilistic visual learning for object detection. Technical Report 326, MIT, June 1995.

[18] J.M. Rehg. *Visual Analysis of High DOF Articulated Objects with Application to Hand Tracking*. PhD thesis, Electrical and Computer Eng., Carnegie Mellon University, 1995.

[19] Romer Rosales, Vassilis Athitsos, Leonid Sigal, and Stan Sclaroff. 3D hand pose reconstruction using specialized mappings. In *ICCV*, volume 1, pages 378–385, 2001.

[20] H. Sagawa and M. Takeuchi. A method for recognizing a sequence of sign language words represented in a japanese sign language sentence. In *Face and Gesture Recognition*, pages 434–439, 2000.

[21] Nobutaka Shimada, Kousuke Kimura, and Yoshiaki Shirai. Real-time 3-D hand posture estimation based on 2-D appearance retrieval using monocular camera. In *Recognition, Analysis and Tracking of Faces and Gestures in Realtime Systems*, pages 23–30, 2001.

[22] M.J. Swain and D.H. Ballard. Color indexing. *IJCV*, 7(1):11–32, 1991.

[23] J. Triesch and C. von der Malsburg. Robotic gesture recognition. In *Gesture Workshop*, pages 233–244, 1997.

[24] A. Utsumi and J. Ohya. Multiple-hand-gesture tracking using multiple cameras. In *CVPR*, volume 1, pages 473–478, 1999.

[25] Virtual Technologies, Inc., Palo Alto, CA. *VirtualHand Software Library Reference Manual*, August 1998.

[26] Y. Wu and T.S. Huang. View-independent recognition of hand postures. In *CVPR*, volume 2, pages 88–94, 2000.

[27] Ying Wu, J.Y. Lin, and T.S. Huang. Capturing natural hand articulation. In *ICCV*, volume 2, pages 426–432, 2001.